Supporting Information:
Electrocatalytic Alcohol Oxidation with Ruthenium Transfer Hydrogenation Catalysts

Kate M. Waldie, Kristen R. Flajslik, Elizabeth McLoughlin, Christopher E. D. Chidsey, Robert M. Waymouth

Department of Chemistry
Stanford University
Stanford CA 94305

Corresponding Author: waymouth@stanford.edu

Contents

^{1}H NMR Spectrum of 3

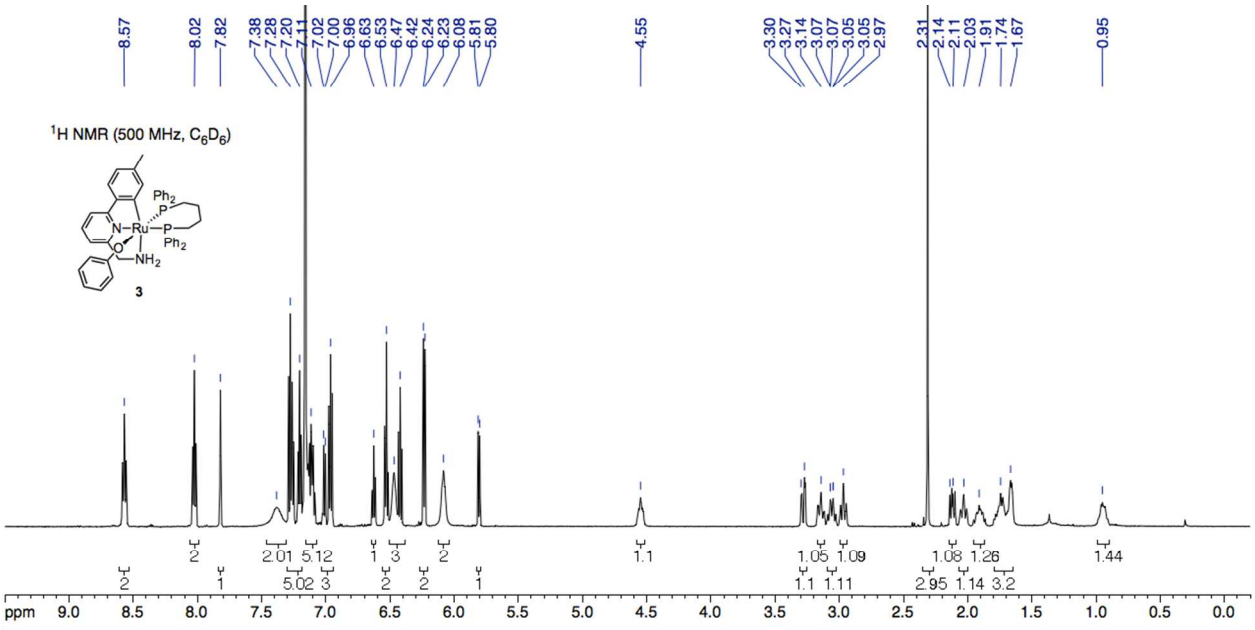

Figure S1. ^{1}H NMR of **3** in C_6D_6.

X-Ray Data and Structures

Table S1. Summary of Crystallographic data for **3**.

empirical formula	$C_{52.25}H_{52}N_2OP_2Ru$	Z	4
formula weight	886.97	D_{calcd} (g/cm^3)	1.283
temp (K)	120(2)	μ (mm^{-1})	0.450
wavelength (Å)	0.71073	F(000)	1846.0
cryst syst	monoclinic	crystal dimens (μm)	250 x 220 x 110
space group	$P2_1/c$	2θ range (deg)	2.88-52.88
a (Å)	10.9808(6)	reflections collected	58927
b (Å)	14.8133(8)	unique reflections	9420
c (Å)	28.4694(15)	no. of parameters	516
α (deg)	90	GOF	1.068
β (deg)	97.3110(10)	R1 [$I > 2\sigma(I)$]	0.0510
γ (deg)	90	wR2 (all data)	0.1561
V (Å^3)	4593.2(4)		

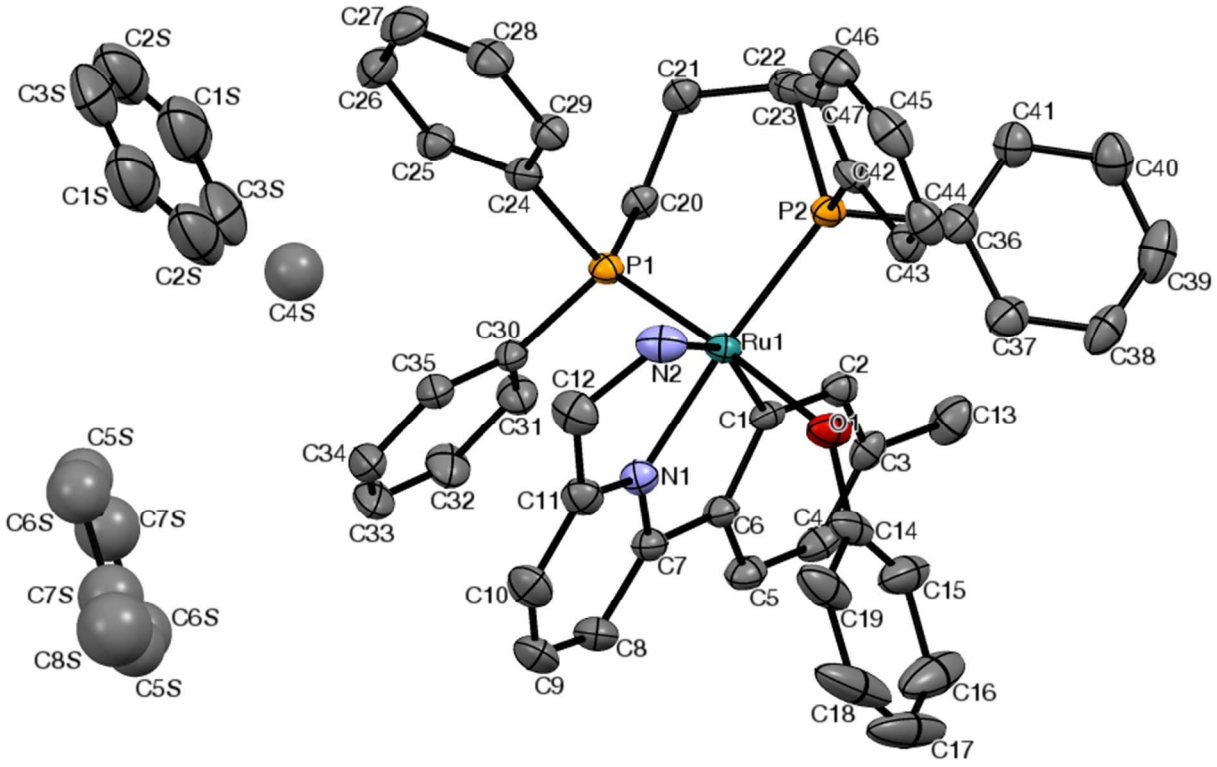

Figure S2. ORTEP and atom-labeling scheme for **3**. Hydrogen atoms are omitted for clarity. Ellipsoids shown at 50% probability.

Transfer Hydrogenation Studies

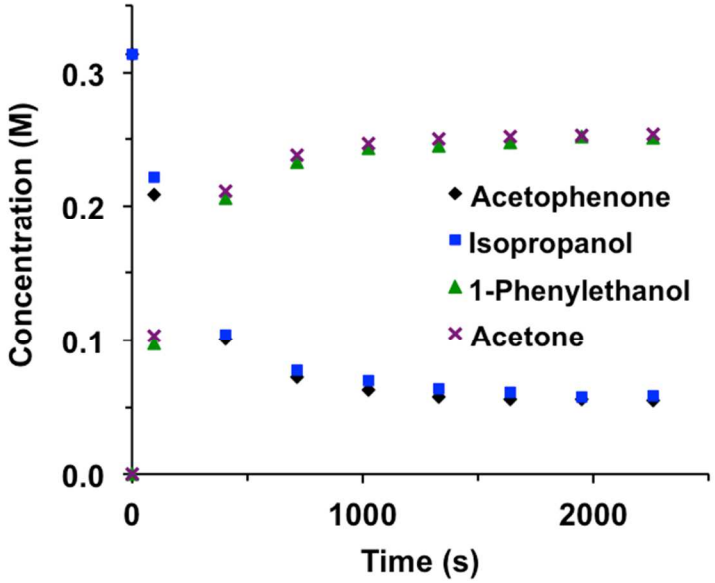

Figure S3. Transfer hydrogenation of acetophenone (0.3 M) with isopropanol (3.1 M) using the Ru-chloride **1** (0.4 mol%) showing the conversion of both reactants and both products, as determined by ^{1}H NMR.

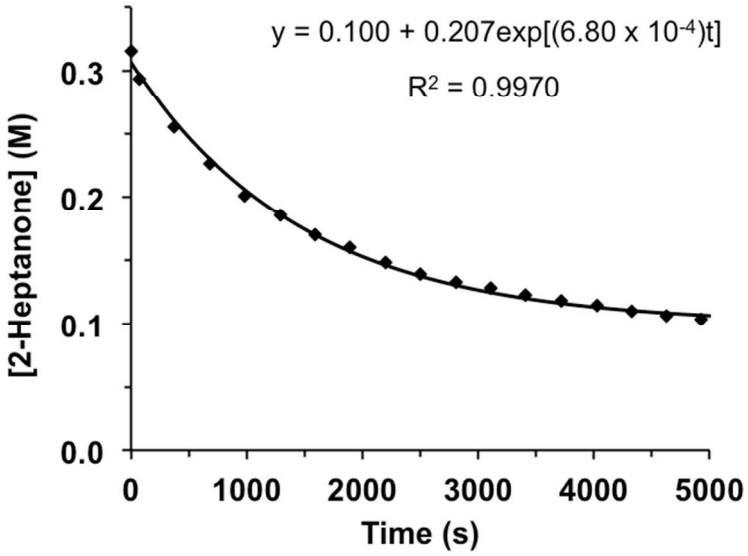

Figure S4. Conversion of 2-heptanone over time and calculated pseudo-first order fit for the transfer hydrogenation of 2-heptanone (0.32 M) with isopropanol-d_8 (3.16 M) in tetrahydrofuran-d_8 using the Ru-hydride **2** (0.63 mM).

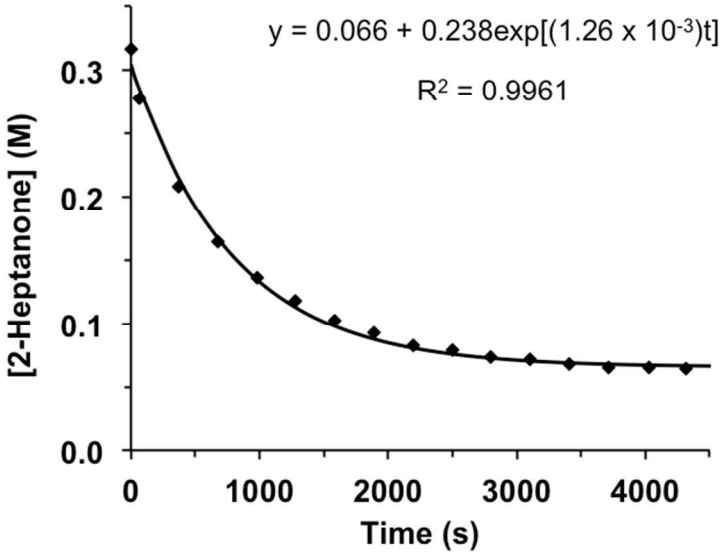

Figure S5. Conversion of 2-heptanone over time and calculated pseudo-first order fit for the transfer hydrogenation of 2-heptanone (0.32 M) with isopropanol-d_8 (3.16 M) in tetrahydrofuran-d_8 using the Ru-hydride **2** (1.26 mM).

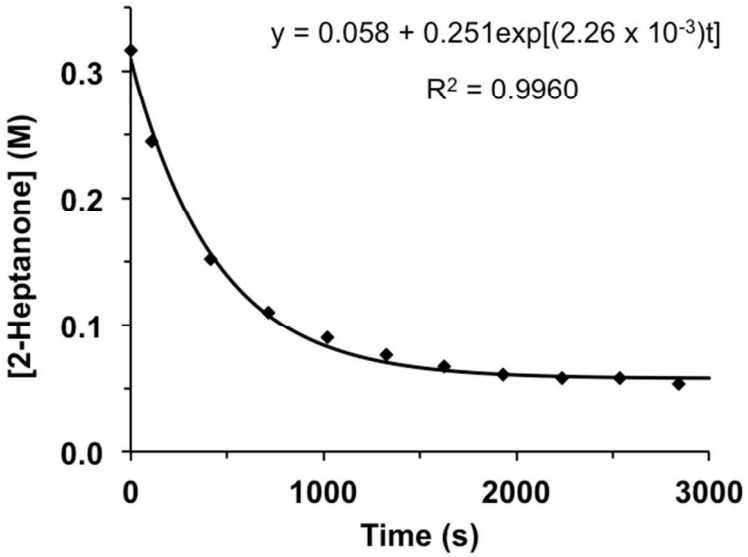

Figure S6. Conversion of 2-heptanone over time and calculated pseudo-first order fit for the transfer hydrogenation of 2-heptanone (0.32 M) with isopropanol-d_8 (3.16 M) in tetrahydrofuran-d_8 using the Ru-hydride **2** (2.53 mM).

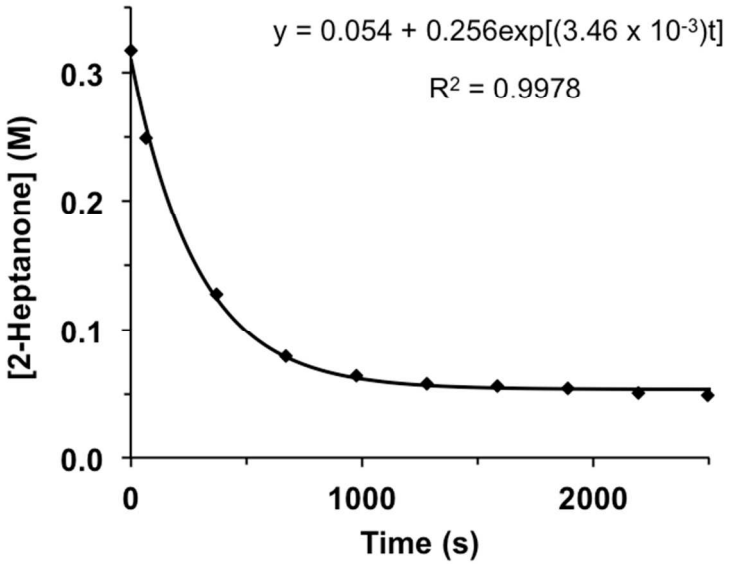

Figure S7. Conversion of 2-heptanone over time and calculated pseudo-first order fit for the transfer hydrogenation of 2-heptanone (0.32 M) with isopropanol-d_8 (3.16 M) in tetrahydrofuran-d_8 using the Ru-hydride **2** (3.67 mM).

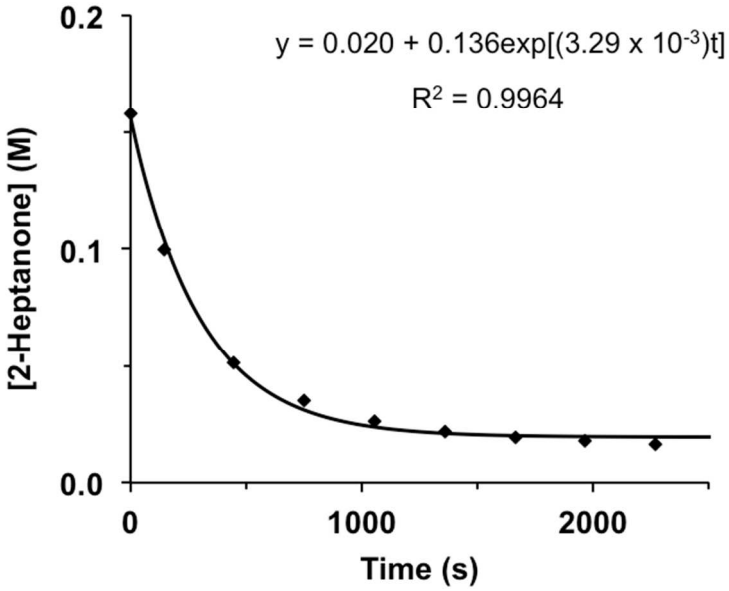

Figure S8. Conversion of 2-heptanone over time and calculated pseudo-first order fit for the transfer hydrogenation of 2-heptanone (0.16 M) with isopropanol-d_8 (9.28 M) in tetrahydrofuran-d_8 using the Ru-hydride **2** (1.26 mM).

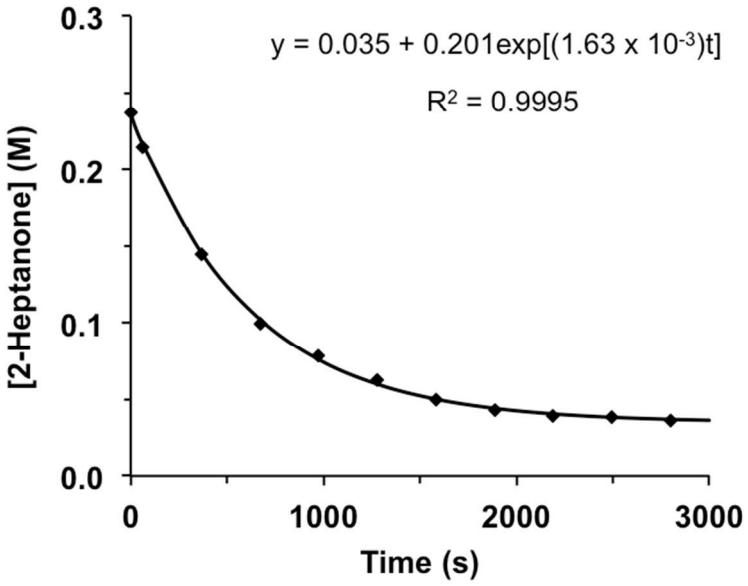

Figure S9. Conversion of 2-heptanone over time and calculated pseudo-first order fit for the transfer hydrogenation of 2-heptanone (0.24 M) with isopropanol-d_8 (9.28 M) in tetrahydrofuran-d_8 using the Ru-hydride **2** (1.26 mM).

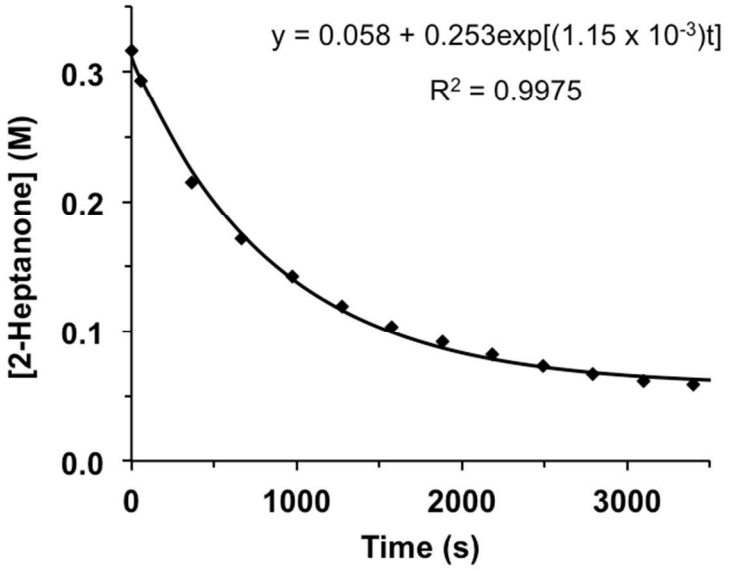

Figure S10. Conversion of 2-heptanone over time and calculated pseudo-first order fit for the transfer hydrogenation of 2-heptanone (0.32 M) with isopropanol-d_8 (9.28 M) in tetrahydrofuran-d_8 using the Ru-hydride **2** (1.26 mM).

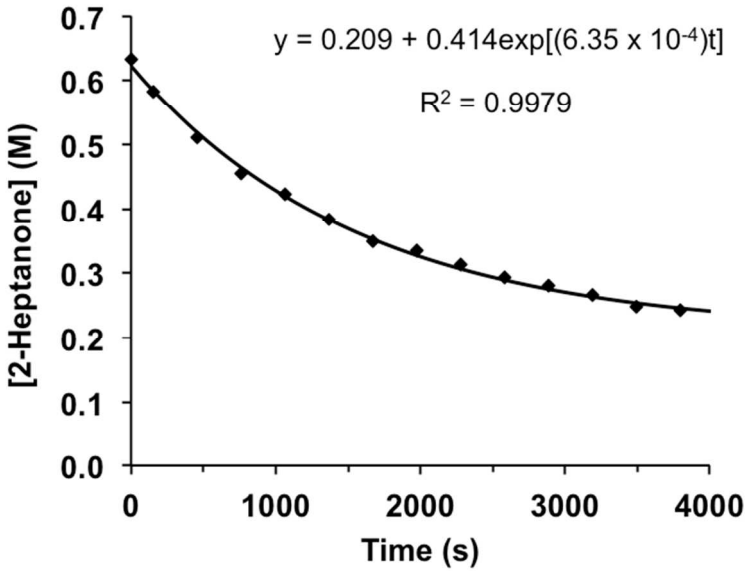

Figure S11. Conversion of 2-heptanone over time and calculated pseudo-first order fit for the transfer hydrogenation of 2-heptanone (0.63 M) with isopropanol-d_8 (9.28 M) in tetrahydrofuran-d_8 using the Ru-hydride **2** (1.26 mM).

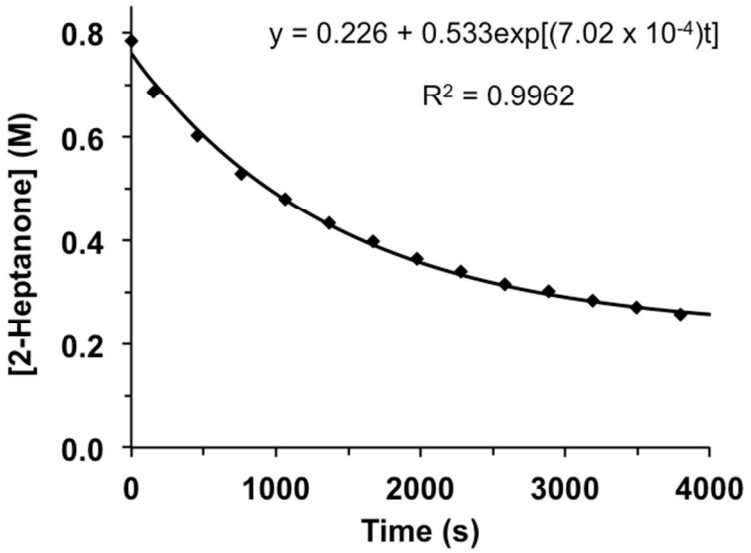

Figure S12. Conversion of 2-heptanone over time and calculated pseudo-first order fit for the transfer hydrogenation of 2-heptanone (0.78 M) with isopropanol-d_8 (9.28 M) in tetrahydrofuran-d_8 using the Ru-hydride **2** (1.26 mM).

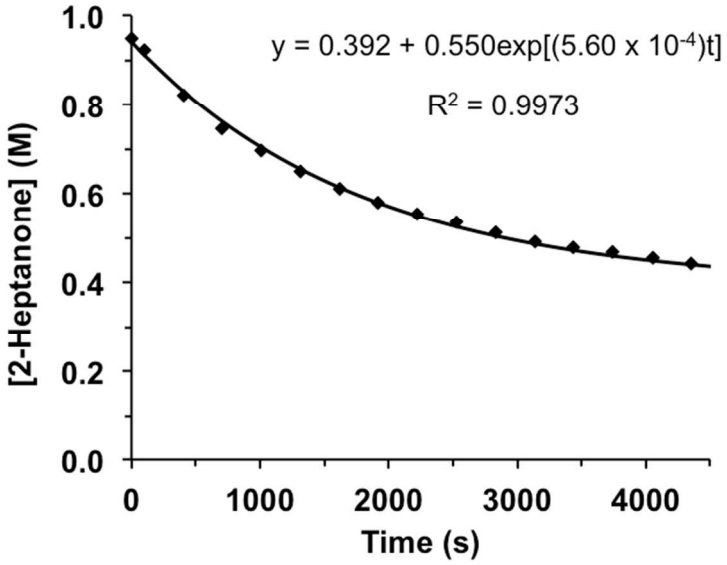

Figure S13. Conversion of 2-heptanone over time and calculated pseudo-first order fit for the transfer hydrogenation of 2-heptanone (0.95 M) with isopropanol-d_8 (9.28 M) in tetrahydrofuran-d_8 using the Ru-hydride **2** (1.26 mM).

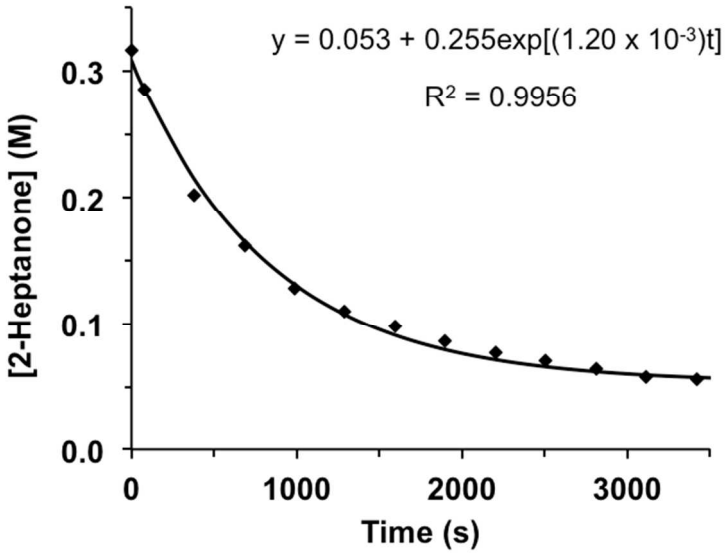

Figure S14. Conversion of 2-heptanone over time and calculated pseudo-first order fit for the transfer hydrogenation of 2-heptanone (0.32 M) with isopropanol-d_8 (4.68 M) in tetrahydrofuran-d_8 using the Ru-hydride **2** (1.26 mM).

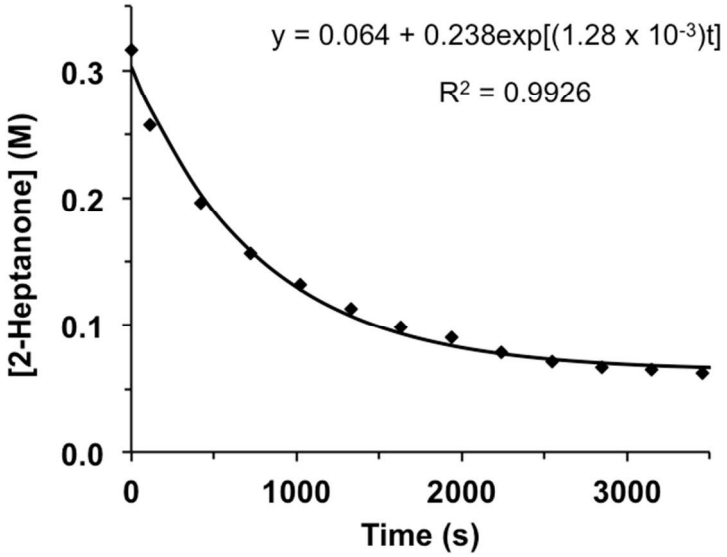

Figure S15. Conversion of 2-heptanone over time and calculated pseudo-first order fit for the transfer hydrogenation of 2-heptanone (0.32 M) with isopropanol-d_8 (6.22 M) in tetrahydrofuran-d_8 using the Ru-hydride **2** (1.26 mM).

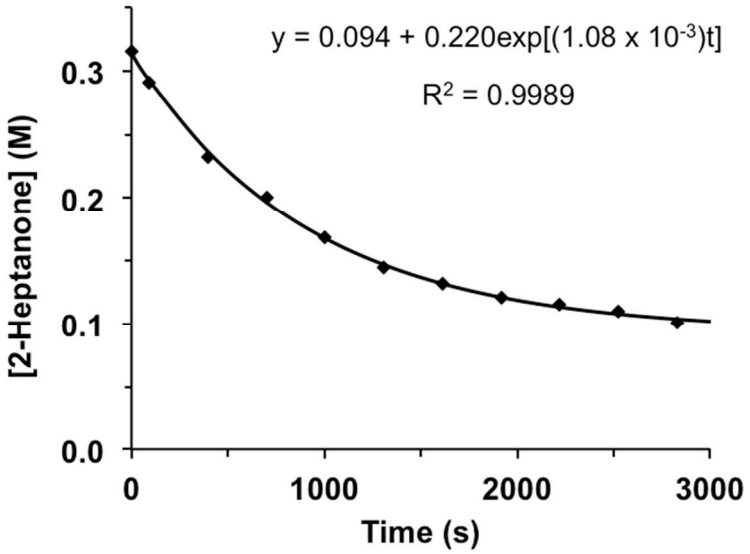

Figure S16. Conversion of 2-heptanone over time and calculated pseudo-first order fit for the transfer hydrogenation of 2-heptanone (0.32 M) with isopropanol-d_8 (3.16 M) and 2-heptanol (0.10 M) in tetrahydrofuran-d_8 using the Ru-hydride **2** (1.26 mM).

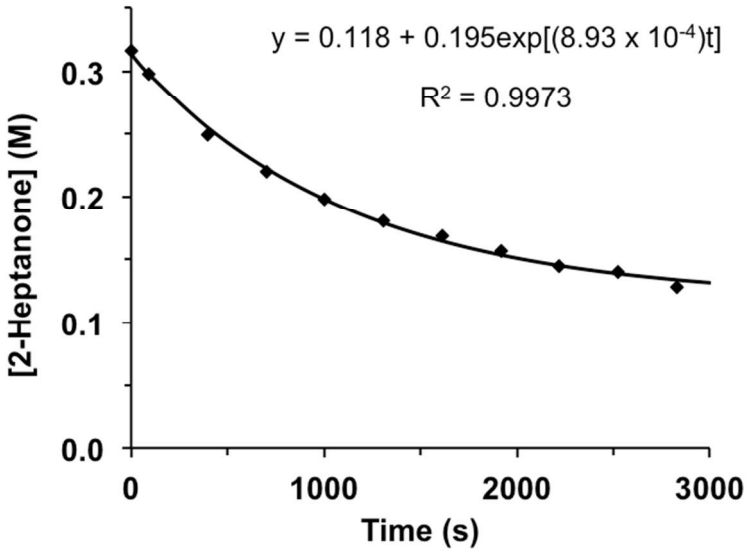

Figure S17. Conversion of 2-heptanone over time and calculated pseudo-first order fit for the transfer hydrogenation of 2-heptanone (0.32 M) with isopropanol-d_8 (3.16 M) and 2-heptanol (0.20 M) in tetrahydrofuran-d_8 using the Ru-hydride **2** (1.26 mM).

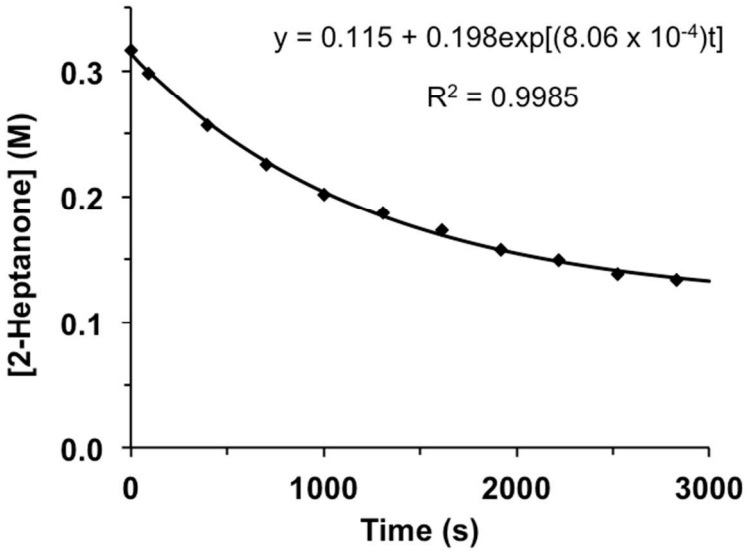

Figure S18. Conversion of 2-heptanone over time and calculated pseudo-first order fit for the transfer hydrogenation of 2-heptanone (0.32 M) with isopropanol-d_8 (3.16 M) and 2-heptanol (0.32 M) in tetrahydrofuran-d_8 using the Ru-hydride **2** (1.26 mM).

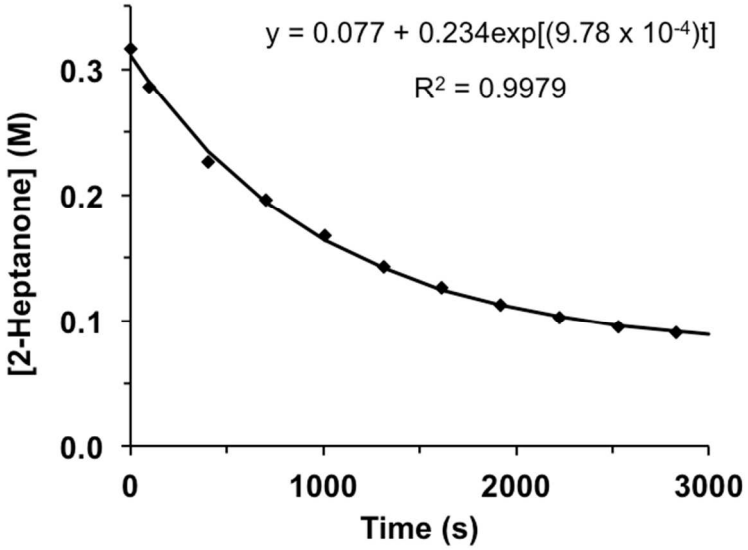

Figure S19. Conversion of 2-heptanone over time and calculated pseudo-first order fit for the transfer hydrogenation of 2-heptanone (0.32 M) with isopropanol-d_8 (3.16 M) and acetone (0.11 M) in tetrahydrofuran-d_8 using the Ru-hydride **2** (1.26 mM).

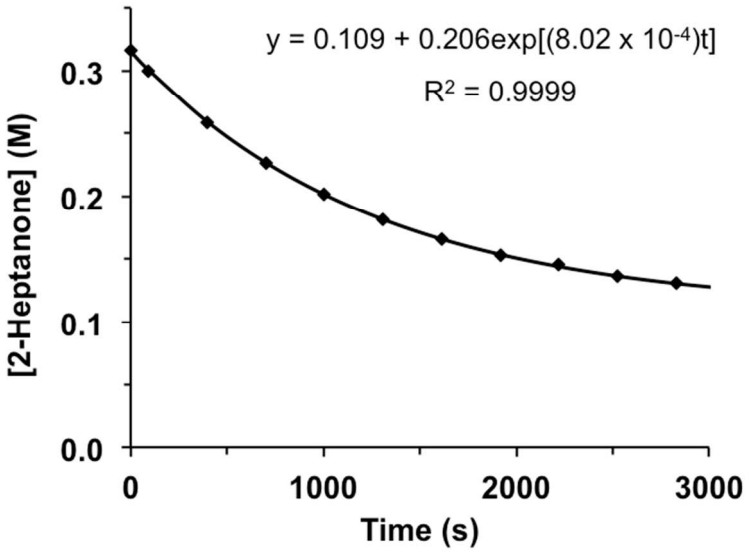

Figure S20. Conversion of 2-heptanone over time and calculated pseudo-first order fit for the transfer hydrogenation of 2-heptanone (0.32 M) with isopropanol-d_8 (3.16 M) and acetone (0.21 M) in tetrahydrofuran-d_8 using the Ru-hydride **2** (1.26 mM).

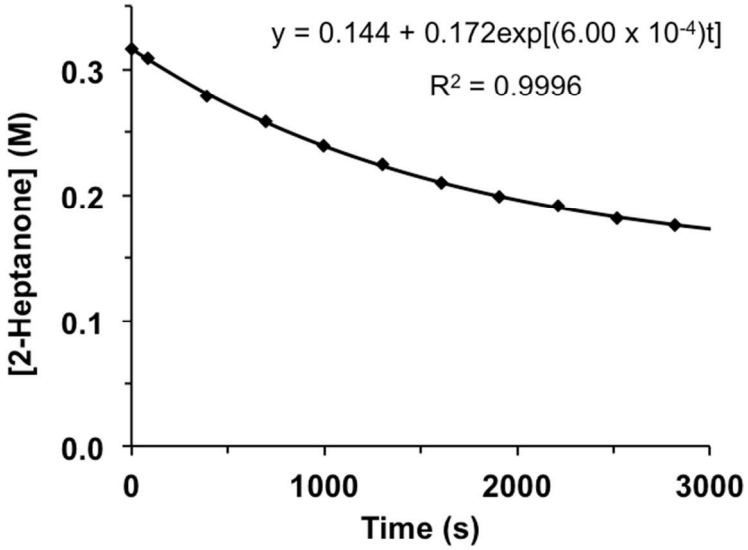

Figure S21. Conversion of 2-heptanone over time and calculated pseudo-first order fit for the transfer hydrogenation of 2-heptanone (0.32 M) with isopropanol-d_8 (3.16 M) and acetone (0.31 M) in tetrahydrofuran-d_8 using the Ru-hydride **2** (1.26 mM).

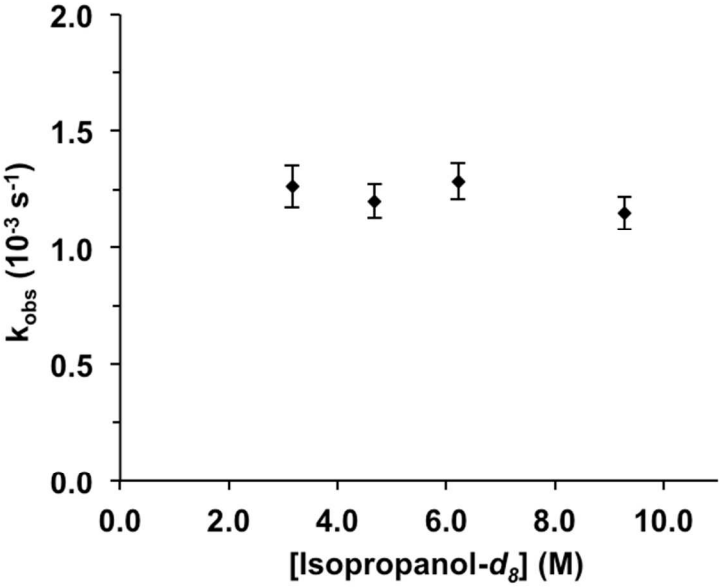

Figure S22. Dependence of k_{obs} on the concentration of isopropanol-d_8 for the transfer hydrogenation of 2-heptanone with isopropanol-d_8 using the Ru-hydride **2**.

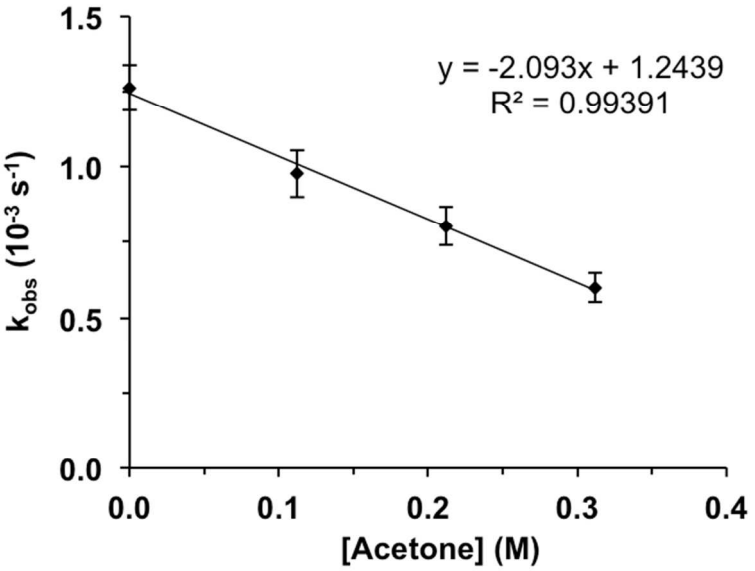

Figure S23. Dependence of k_{obs} on the concentration of acetone for the transfer hydrogenation of 2-heptanone with isopropanol-d_8 using the Ru-hydride **2**.

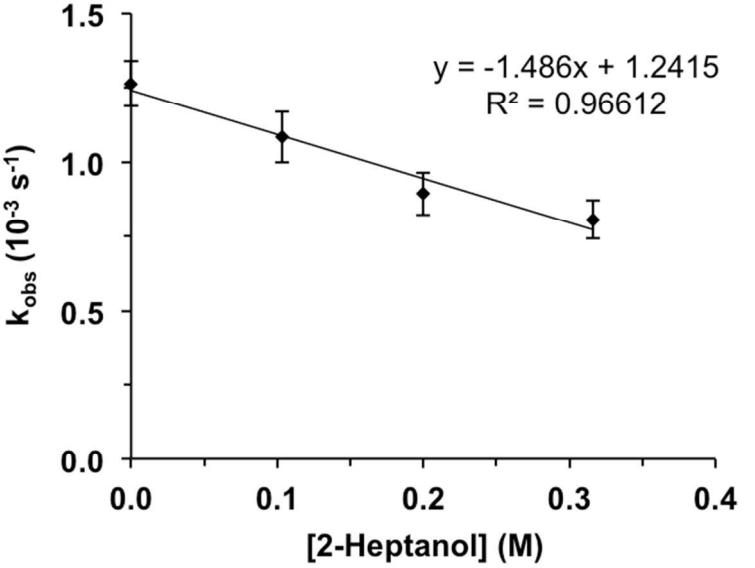

Figure S24. Dependence of k_{obs} on the concentration of 2-heptanol for the transfer hydrogenation of 2-heptanone with isopropanol-d_8 using the Ru-hydride **2**.

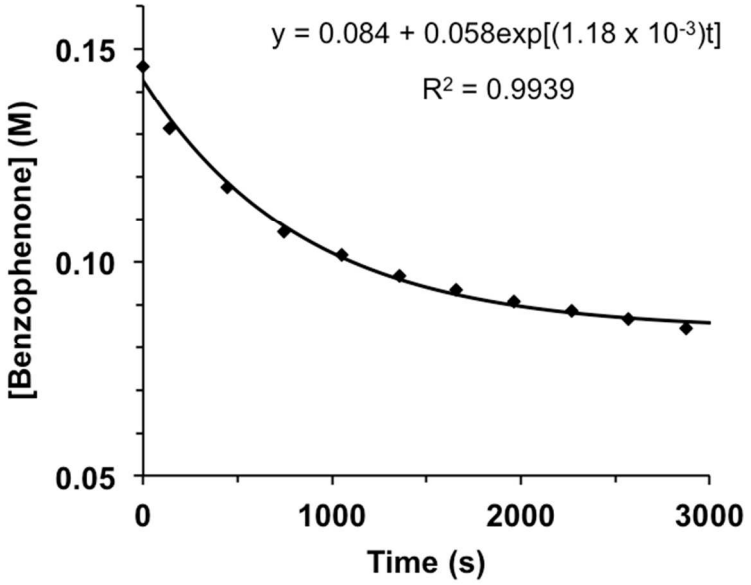

Figure S25. Conversion of benzophenone over time and calculated pseudo-first order fit for the transfer hydrogenation of benzophenone (0.15 M) with isopropanol-d_8 (9.28 M) in tetrahydrofuran-d_8 using the Ru-hydride **2** (1.26 mM).

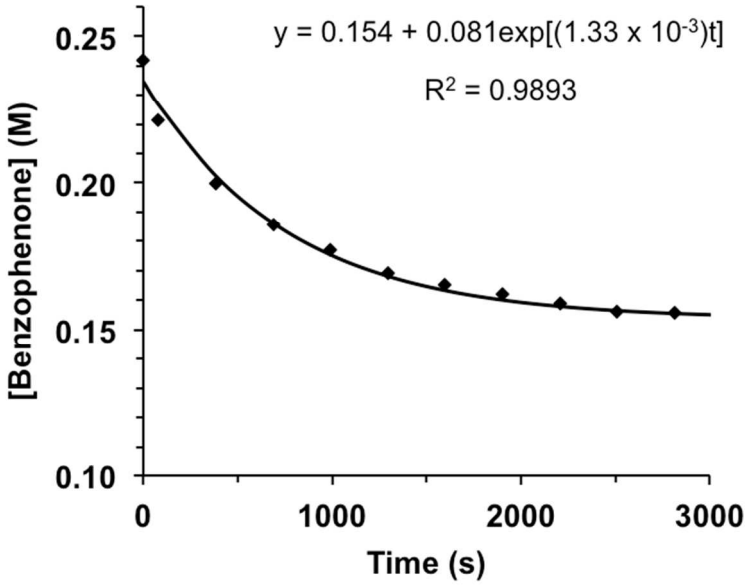

Figure S26. Conversion of benzophenone over time and calculated pseudo-first order fit for the transfer hydrogenation of benzophenone (0.24 M) with isopropanol-d_8 (9.28 M) in tetrahydrofuran-d_8 using the Ru-hydride **2** (1.26 mM).

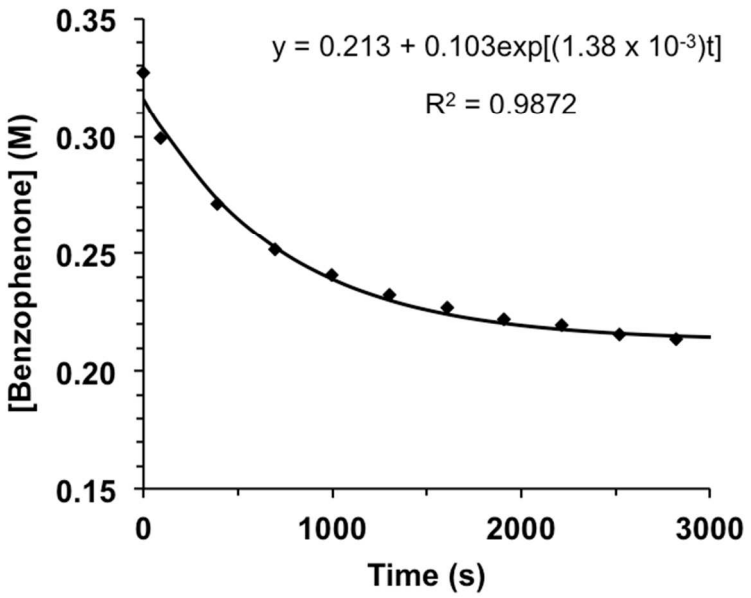

Figure S27. Conversion of benzophenone over time and calculated pseudo-first order fit for the transfer hydrogenation of benzophenone (0.33 M) with isopropanol-d_8 (9.28 M) in tetrahydrofuran-d_8 using the Ru-hydride **2** (1.26 mM).

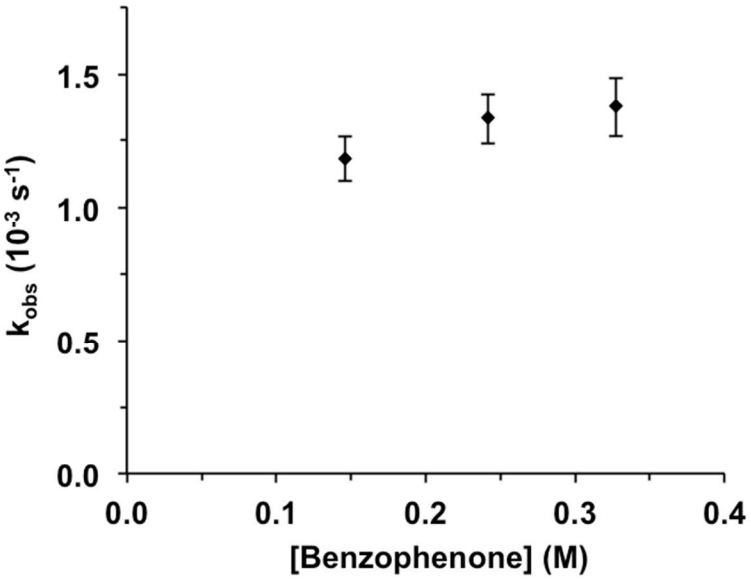

Figure S28. Dependence of k_{obs} on the concentration of benzophenone for the transfer hydrogenation of benzophenone with isopropanol-d_8 using the Ru-hydride **2**.

Additional Cyclic Voltammograms

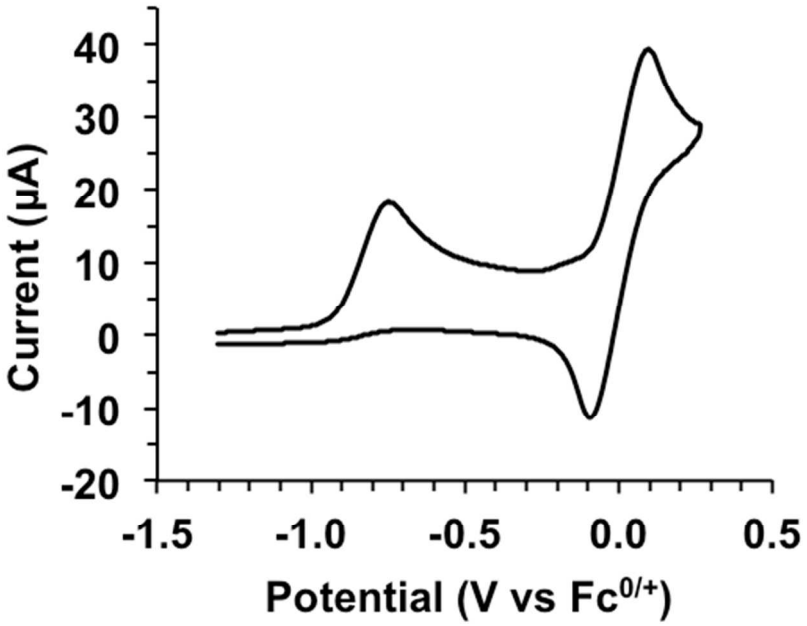

Figure S29. Cyclic voltammogram of **2** in tetrahydrofuran in the presence of equimolar ferrocene, scan rate 100 mVs.

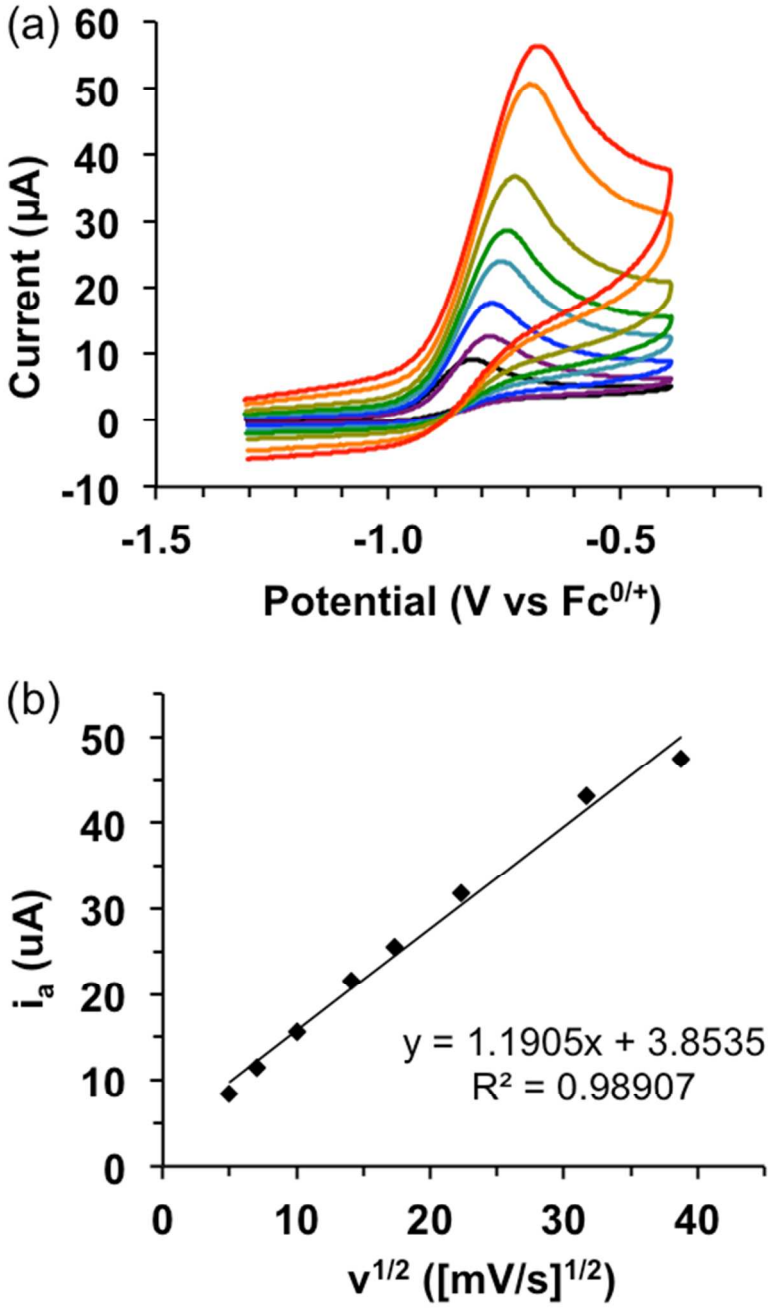

Figure S30. (a) Cyclic voltammograms of **2** in tetrahydrofuran (1.2 mM Ru) at various scan rates: 25 mV/s (black), 50 mV/s (purple), 100 mV/s (blue), 200 mV/s (cyan), 300 mV/s (green), 500 mV/s (gold), 1 V/s (orange), 1.5 V/s (red). (b) Square root of the scan rate dependence on the maximum peak current i_a.

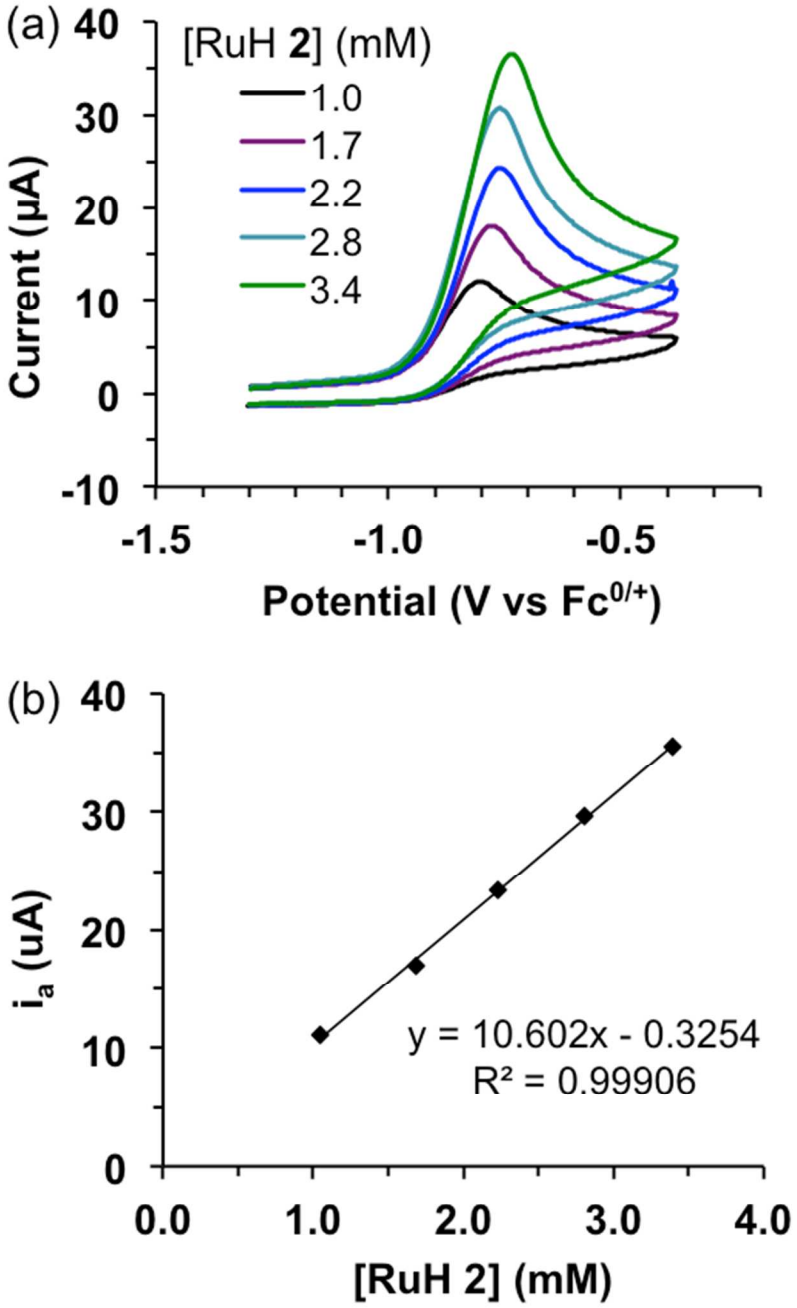

Figure S31. (a) Cyclic voltammograms of the Ru-hydride **2** in tetrahydrofuran, followed by further addition of **2** at 100 mV/s scan rate. (b) [**2**] dependence on the maximum peak current i_a.

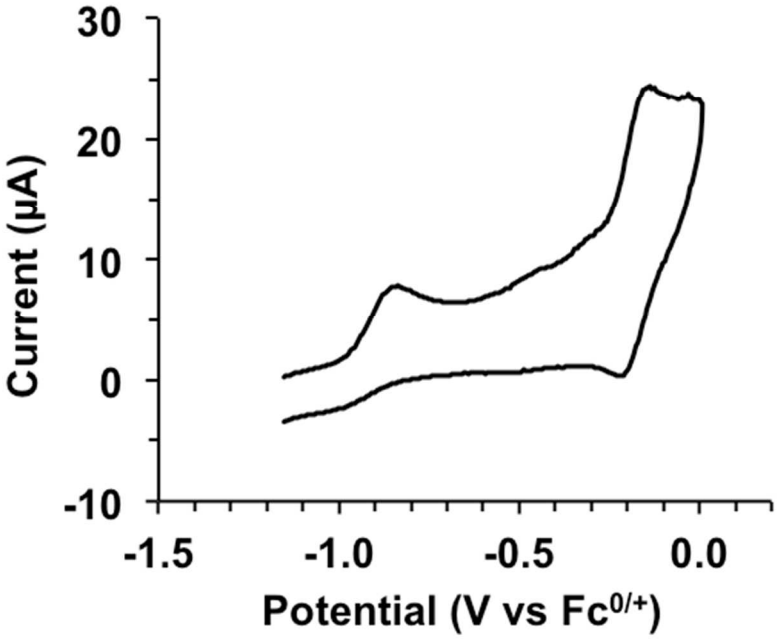

Figure S32. Larger window cyclic voltammogram of **2** in tetrahydrofuran, scan rate 100 mV/s.

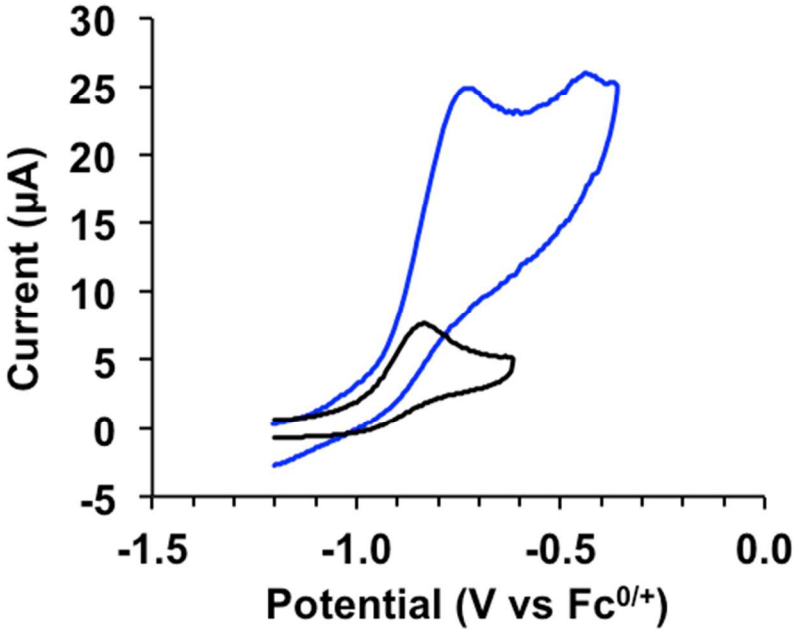

Figure S33. Cyclic voltammograms of **2** in tetrahydrofuran without isopropanol (black trace) and with 0.10 M isopropanol (blue trace). Scan rate 100 mV/s.

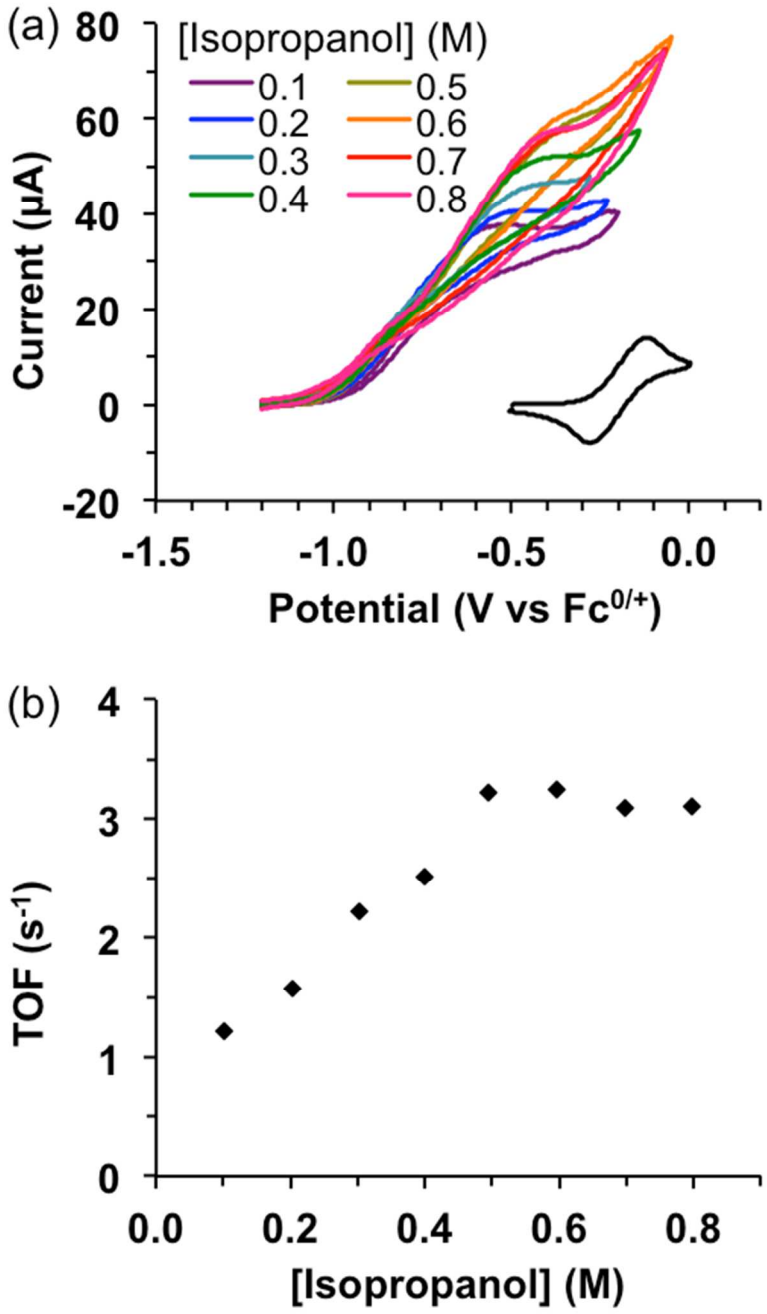

Figure S34. (a) Cyclic voltammograms of **1** (1 mM Ru) in tetrahydrofuran (black), followed by addition of potassium *t*-butoxide (15 mM) and titration of isopropanol at 100 mV/s scan rate. (b) [Isopropanol] dependence on the turnover frequency.

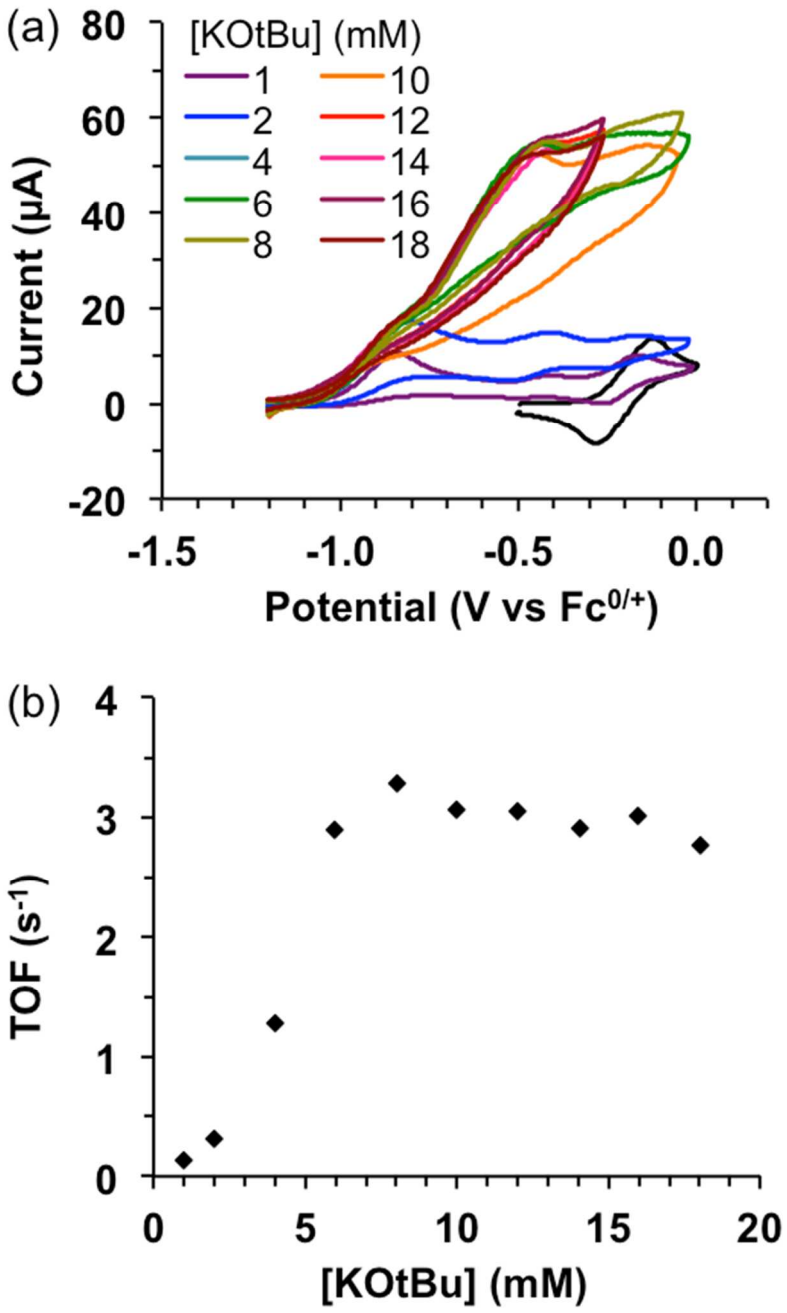

Figure S35. (a) Cyclic voltammograms of **1** (1 mM Ru) and isopropanol (0.50 M) in tetrahydrofuran (black), followed by titration of potassium *t*-butoxide at 100 mV/s scan rate. (b) [KOtBu] dependence on the turnover frequency.

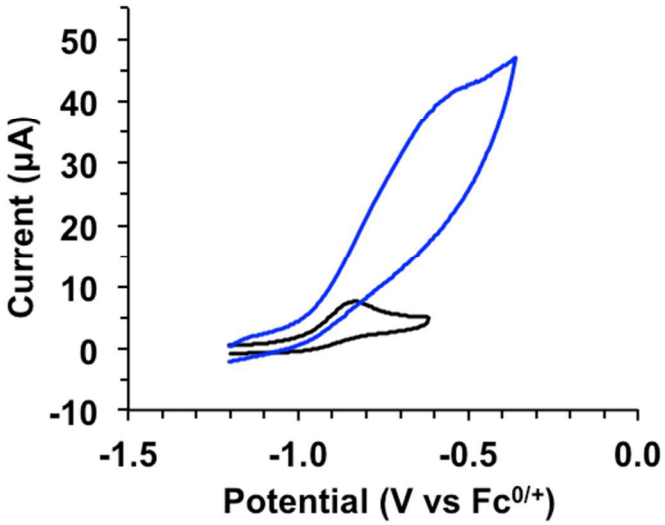

Figure S36. Cyclic voltammograms of **2** (1 mM Ru) in tetrahydrofuran (black) and with 20 mM potassium *t*-butoxide and 0.5 M isopropanol (blue). Scan rate 100 mV/s.

Chemical Oxidation of the Ru-hydride 2

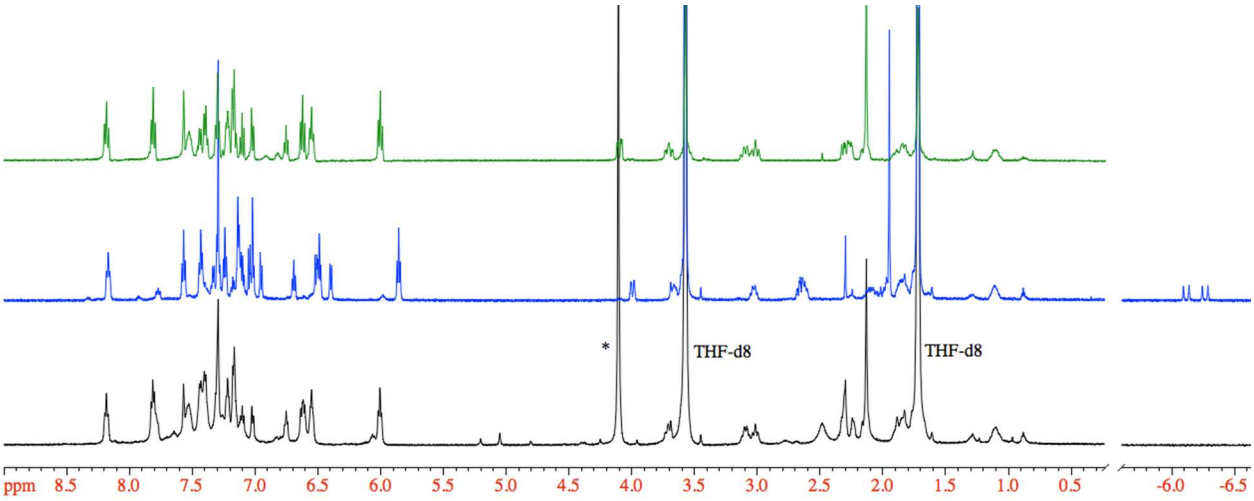

Figure S37. ^{1}H NMR spectra in tetrahydrofuran-d_8 of the Ru-chloride **1** (top spectrum, green), the Ru-hydride **2** (middle spectrum, blue), and the reaction mixture from oxidation of **2** with one equivalent of ferrocenium tetrafluoroborate (bottom spectrum, black). Ferrocene marked by asterisk.

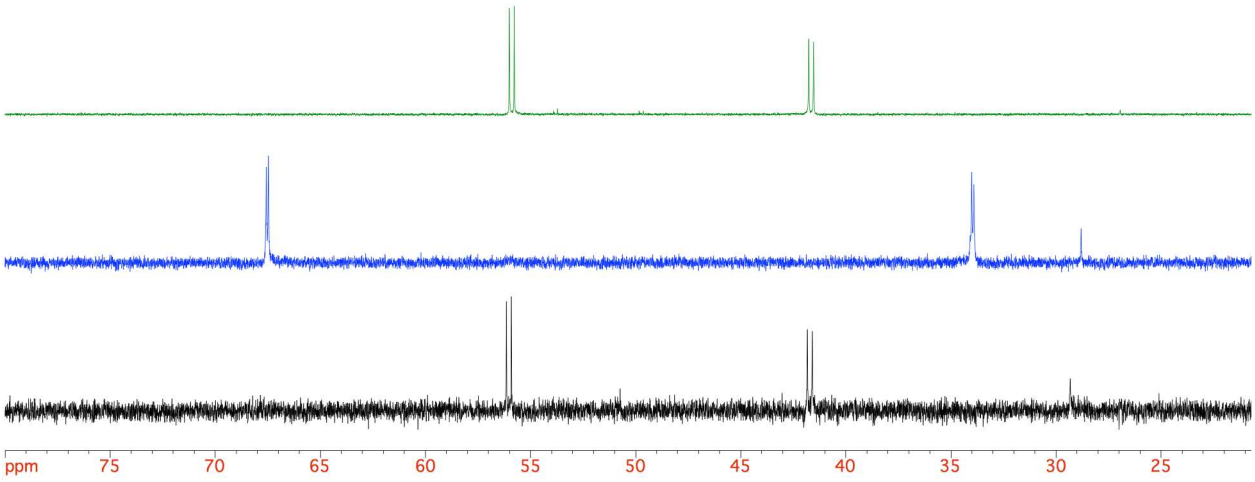

Figure S38. ^{31}P NMR spectra in tetrahydrofuran-d_8 of the Ru-chloride **1** (top spectrum, green), the Ru-hydride **2** (middle spectrum, blue), and the reaction mixture from oxidation of **2** with one equivalent of ferrocenium tetrafluoroborate (bottom spectrum, black).

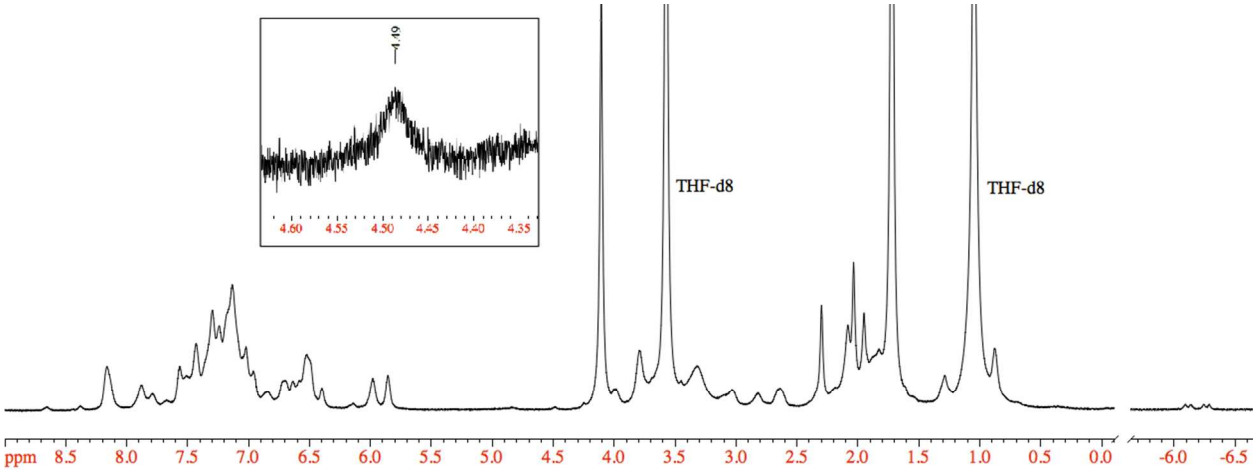

Figure S39. ^{1}H NMR spectra in tetrahydrofuran-d_8 of the Ru-hydride **2** (13.8 mM) treated with half an equivalent of ferrocenium tetrafluoroborate (6.6 mM). *Inset*: Singlet peak from H_2 evolution.

The concentration of dissolved hydrogen in this reaction mixture (1 mL solution volume) was quantified by ^{1}H NMR by integration of the dihydrogen singlet peak compared that to ferrocene. The dissolved H_2 concentration C_{Soln} was thus determined to be 0.17 mM. The total mmol of H_2 produced N_{H2} is given by the sum of the mmol of H_2 dissolved in solution and the mmol of H_2 in the headspace:

$$N_{H2} = N_{H2,Soln} + N_{H2,Headspace} \qquad (1)$$

Using Henry's Law constant k_H for H_2 in tetrahydrofuran (3.004×10^2 atm·L·mol^{-1}), N_{H2} is:

$$N_{H2} = C_{Soln}V_{Soln} + k_H C_{Soln}\left(\frac{V_G}{RT}\right) \qquad (2)$$

where V_S = solution volume (1.0 mL), V_G = headspace volume (1.5 mL), R = gas constant, and T = temperature. The total mmol of H_2 produced was thus calculated to be 0.00336 mmol, which is 97% of the theoretical value of 0.00344 mmol H_2 for the oxidation of **2** with 0.5 equivalents of ferrocenium tetrafluoroborate.

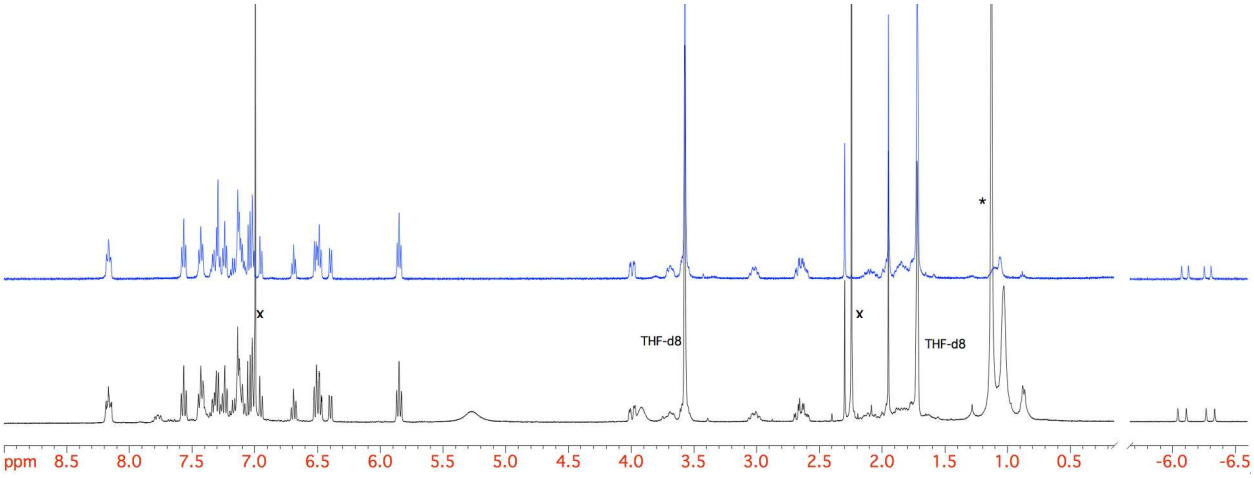

Figure S40. ^{1}H NMR spectra in tetrahydrofuran-d_8 of the Ru-hydride **2** (top spectrum, blue), followed by addition of one equivalent of potassium *t*-butoxide (bottom spectrum, black). Potassium *t*-butoxide marked by asterisk, and *p*-xylene internal standard marked by x.

Controlled Potential Electrolysis Studies

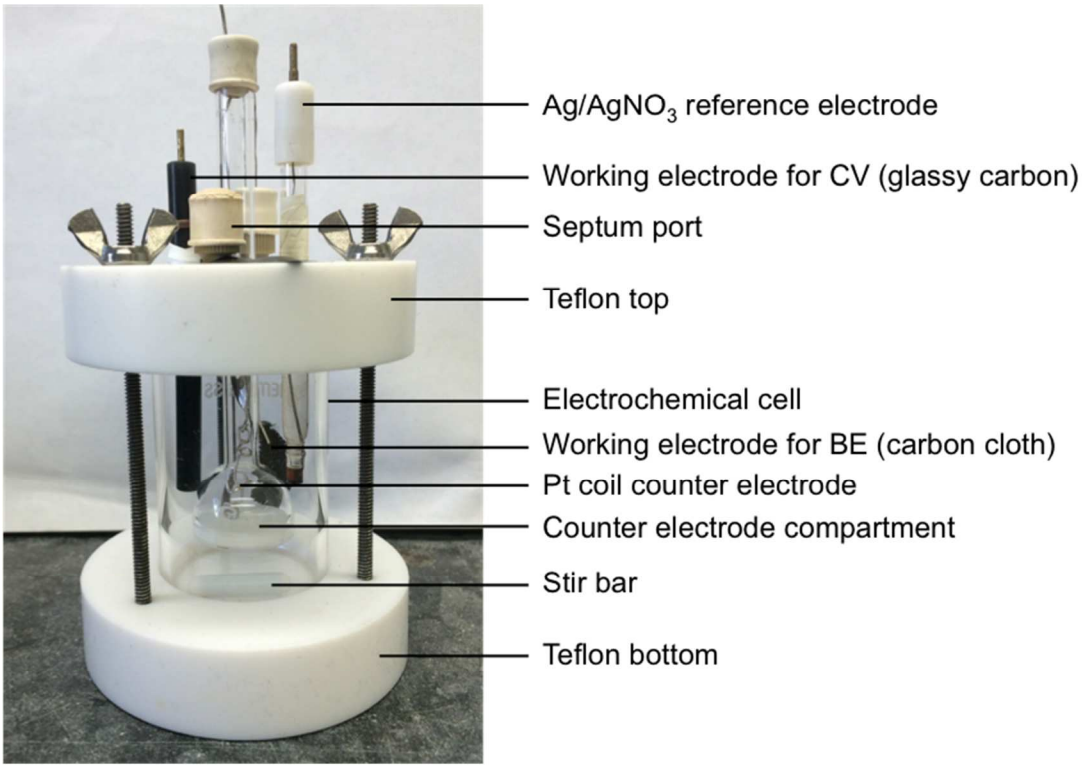

Figure S41. Picture of the custom large-volume cell for controlled potential electrolysis.

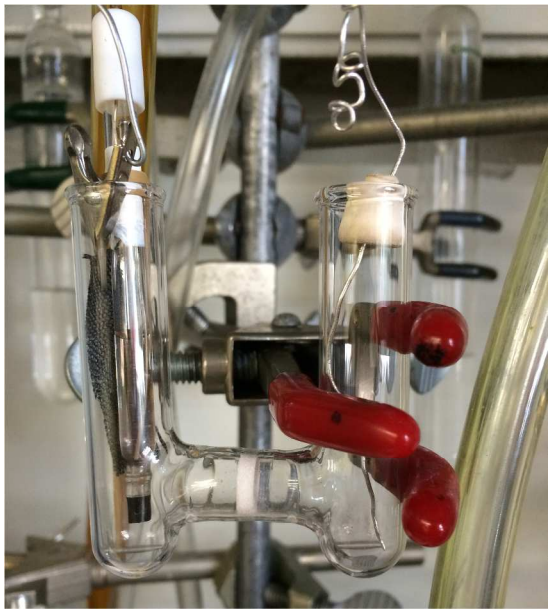

Figure S42. Picture of the small-volume H-cell for controlled potential electrolysis.

*Exhaustive Oxidation of **2***. The small-volume electrolysis H-cell containing the carbon cloth working electrode and $Ag/AgNO_3$ reference electrode was charged with 2.2 mL of 0.5 mM [RuH(CNN)(dppb)] **2** in 0.1 M Bu_4NPF_6 in acetonitrile. The auxiliary electrode compartment was filled with electrolyte solution at the same concentration. Controlled potential electrolysis was performed at -0.60 V versus $Fc^{0/+}$. The charge passed during the electrolysis was 0.096 C, determined by integration of the current versus time curve (Figure S43). This value is in good agreement with 0.106 C, the theoretical total charge passed for the one-electron oxidation of **2** calculated according to:

$$Q = nFN_2$$

where n = number of electrons, F = Faraday's constant, and N_2 = moles of **2**.

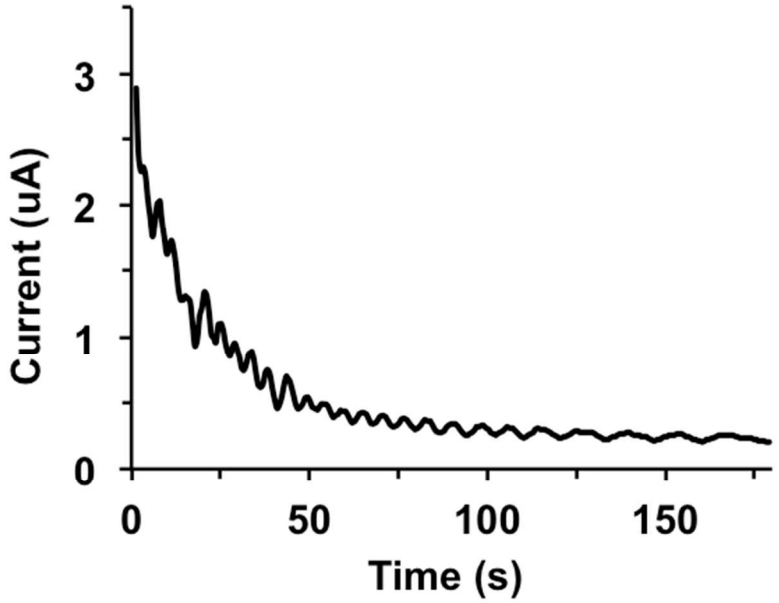

Figure S43. Controlled-potential electrolysis of **2** in acetonitrile (0.5 mM Ru in 0.1 M Bu_4NPF_6) at -0.60 V versus $Fc^{0/+}$.

*Exhaustive Oxidation of **2** in the Presence of Base.* The custom large-volume electrolysis cell containing the carbon cloth working electrode and $Ag/AgNO_3$ reference electrode was charged with 20.0 mL of 0.8 mM [RuH(CNN)(dppb)] **2** in 0.1 M Bu_4NPF_6 with 0.03 M potassium *t*-butoxide in 1:1 tetrahydrofuran/1,2-difluorobenzene. The auxiliary electrode compartment was filled with electrolyte solution at the same concentration. Controlled potential electrolysis was performed at -0.6 V versus $Fc^{0/+}$. The charge passed during the electrolysis was 3.11 C, determined by integration of the current versus time curve (Figure S44). This value is in good agreement with 3.19 C, the theoretical total charge passed for the two-electron, one-proton oxidation of **2** in the presence of base calculated according to:

$$Q = nFN_2$$

where n = number of electrons, F = Faraday's constant, and N_2 = moles of **2**.

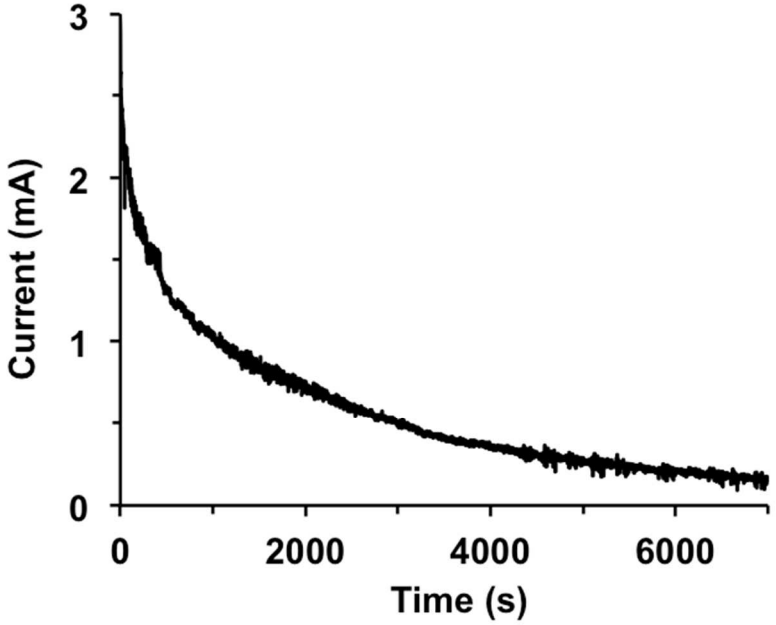

Figure S44. Controlled-potential electrolysis of **2** with 0.03 M potassium *t*-butoxide in 1:1 tetrahydrofuran/1,2-difluorobenzene (0.8 mM Ru in 0.1 M Bu_4NPF_6) at -0.6 V versus $Fc^{0/+}$.

*Electrocatalytic Activity with **1***. The custom large-volume electrolysis cell containing the carbon cloth working electrode and $Ag/AgNO_3$ reference electrode was charged with 15.5 mL of 0.5 mM [RuCl(CNN)(dppb)] **1** in 0.1 M Bu_4NPF_6 with 0.4 M isopropanol and 0.02 M potassium *t*-butoxide in 1:1 tetrahydrofuran/1,2-difluorobenzene. The auxiliary electrode compartment was filled with electrolyte solution at the same concentration. Controlled potential electrolysis was performed at -0.6 V versus $Fc^{0/+}$ for one hour. The charge passed during the electrolysis was 7.34 C, determined by integration of the current versus time curve (Figure S45). The theoretical acetone production for this charge Q is 0.038 mmol using the following equation:

$$Q = nFN_{acetone}$$

where n = number of electrons, F = Faraday's constant, and $N_{acetone}$ = moles acetone.

Acetone production was quantified by gas chromatographic analysis of the working compartment solution using 1-butanol as an internal standard. The actual mmol of acetone produced was determined to be 0.036 mmol. The Faradaic efficiency for acetone production is thus 94 ± 5 %.

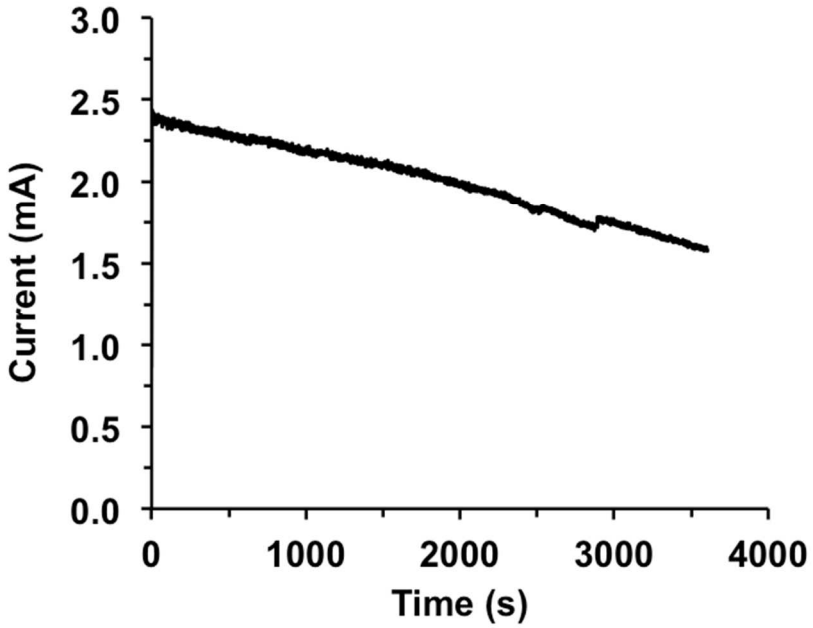

Figure S45. Controlled-potential electrolysis of **1** with 0.4 M isopropanol and 0.02 M potassium *t*-butoxide in 1:1 tetrahydrofuran/1,2-difluorobenzene (0.5 mM Ru in 0.1 M Bu_4NPF_6) at -0.6 V versus $Fc^{0/+}$.

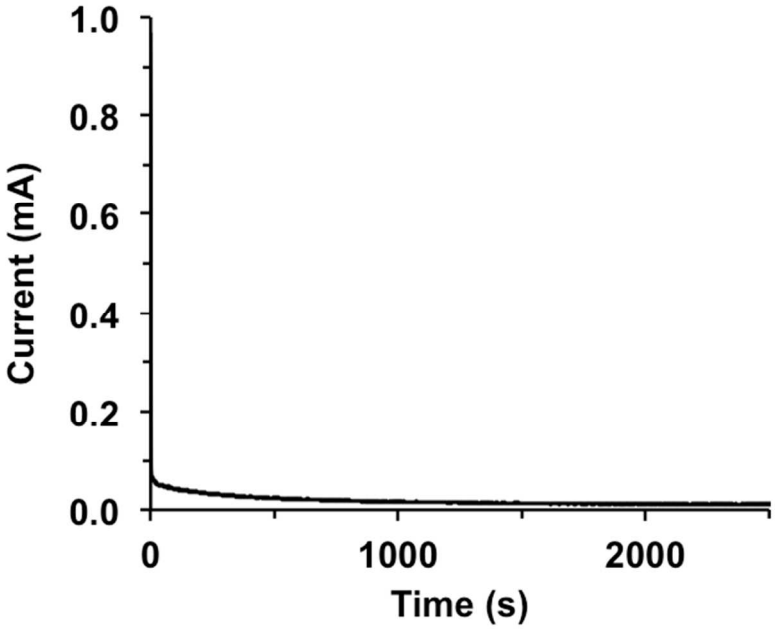

Figure S46. Controlled-potential electrolysis of 0.4 M isopropanol and 0.02 M potassium *t*-butoxide in 1:1 tetrahydrofuran/1,2-difluorobenzene (0.1 M Bu_4NPF_6) in the absence of Ru catalyst at -0.6 V versus $Fc^{0/+}$.